

Thermoelectrics in an array of molecular junctions

K.-H. Müller^{a)}

CSIRO Materials Science and Engineering, P.O. Box 218, Lindfield, New South Wales 2070, Australia

(Received 25 October 2007; accepted 6 June 2008; published online 30 July 2008)

The room temperature thermoelectric properties of a three-dimensional array of molecular junctions are calculated. The array is composed of n -doped silicon nanoparticles where the surfaces are partially covered with polar molecules and the nanoparticles are bridged by *trans*-polyacetylene molecules. The role of the polar molecules is to reduce the band bending in the n -doped silicon nanoparticles and to shift the electronic resonances of the bridging molecules to the nanoparticle conduction band edges where the molecular resonances act as electron energy filters. The transmission coefficients of the bridging molecules that appear in the formulas for the Seebeck coefficient, the electrical conductance, and the electronic thermal conductance, are calculated using the nonequilibrium Green's function technique. A simple tight-binding Hamiltonian is used to describe the bridging molecules, and the self-energy term is calculated using the parabolic conduction band approximation. The dependencies of the thermoelectric properties of the molecular junctions on the silicon doping concentration and on the molecule-nanoparticle coupling are discussed. The maximal achievable thermoelectric figure of merit ZT of the array is estimated as a function of the phononic thermal conductance of the bridging molecules and the doping of the nanoparticles. The power factor of the array is also calculated. For sufficiently small phononic thermal conductances of the bridging molecules, very high ZT values are predicted. © 2008 American Institute of Physics. [DOI: 10.1063/1.2953462]

I. INTRODUCTION

During the past 50 years, a great deal of research effort has gone into the development of thermoelectric materials with high efficiency and their application in devices to convert thermal energy into electrical energy and in reverse to perform refrigeration.^{1,2} The efficiency η of a thermoelectric material is given by³

$$\eta = \eta_c \frac{\sqrt{1+ZT} - 1}{\sqrt{1+ZT} + T_C/T_H}, \quad (1)$$

where η_c is the Carnot efficiency which is defined as $\eta_c = 1 - T_C/T_H$, T_{CH} are the cold/hot reservoir temperatures with average temperature $T \equiv (T_C + T_H)/2$, and ZT is the important thermoelectric figure of merit which is defined as

$$ZT = \frac{S^2 G}{\kappa} T. \quad (2)$$

In Eq. (2), the quantity S is the Seebeck coefficient (thermopower), G is the electrical conductance, and κ is the thermal conductance of the material. The thermal conductance is the sum of the electronic thermal conductance κ_e and the phononic thermal conductance κ_{ph} .

$$\kappa = \kappa_e + \kappa_{ph}. \quad (3)$$

As can be seen from Eq. (1), the larger the figure of merit ZT , the more efficient a thermoelectric material becomes. Thus, a good thermoelectric material must have a large ZT which can be achieved with a high Seebeck coefficient S , a

high electrical conductance G , and a low thermal conductance κ . Another thermoelectric quantity commonly of interest is the power factor given by $P = S^2 \sigma$, where σ is the electrical conductivity of the material. A good thermoelectric material should have a large power factor. In the late 1950s bismuth telluride alloys were developed that showed ZT values around 0.5. Between 1960 and 2000 the field of thermoelectric research was quite stagnant with $ZT \approx 1$, and efficiencies of about 10% of the Carnot limit were achieved in some commercial devices using bismuth telluride based alloys. In the early 1990s Hicks and Dresselhaus^{4,5} pointed out in theoretical papers that reducing the dimensionality of a semiconducting material (i.e., in the form of superlattices and nanowires) can enhance the electronic density of states near the Fermi level which is predicted to enhance ZT . In such low dimensional materials, the increase in phonon surface scattering decreases the phononic thermal conductance which further enhances ZT . These calculations were refined later by Sun *et al.*⁶ and it was predicted that Bi nanowires reach a ZT of 1.5 at a wire thickness of 10 nm and that the ZT increases further as the wire gets thinner. Lin *et al.*⁷ predicted ZT values of about 4 and 6 for 5-nm-diameter PbSe/PbS and PbTe/PbSe superlattice wires at 77 K. The theoretical work on nanostructured materials inspired experimentalist to search for nanostructured materials with high ZT values. Harman *et al.*⁸ observed $ZT \approx 1.6$ in a PbSeTe based quantum dot superlattice, Venkatasubramanian *et al.*⁹ achieved $ZT \approx 2.4$ in a p -type Bi₂Te₃/Sb₂Te₃ superlattice, and Hsu *et al.*¹⁰ reported $ZT \approx 2.2$ in alloys containing nanometer sized metallic grains embedded in a semiconducting matrix. Most of these ZT enhancements were attributed

^{a)}Electronic mail: karl.muller@csiro.au.

to lowering the phononic thermal conductance κ_{ph} . Recently, thermoelectric materials made of carbon nanotubes attracted some interest.^{11,12} Also, Lyeo *et al.*¹³ measured the Seebeck coefficient across a junction formed by a semiconducting substrate and the tip of a scanning transmission microscope. The consensus is that finding a material with a thermoelectric figure of merit $ZT \geq 4$ would mark a major technological breakthrough.

Much progress has been made recently in an area called “molecular electronics”¹⁴ where a better understanding has been gained of the thermoelectric properties of single molecules sandwiched between macroscopic metal electrodes.^{16,15}

In this paper we suggest a novel material consisting of a three-dimensional (3D) array of molecular junctions where *trans*-polyacetylene bridging molecules connect *n*-doped silicon nanoparticles. We show by model calculations that high *ZT* values at room temperature can be achieved by exploiting the thermoelectric properties of molecular junctions.

In Sec. II, we derive the equations that determine the thermoelectric figure of merit *ZT* of an array of molecular junctions and introduce the equations that describe the thermoelectric properties of the molecules that form a junction. We give expressions for the transmission coefficient of the bridging molecules, the self-energies and the electrostatic interaction between electrons of the bridging molecule and the polar molecules.

In Sec. III, we comment on the importance of shifting the molecular resonances and on the effect of polar-molecule site-occupation variations. We draw attention to the thermoelectric properties of individual bridging molecules in a junction and show results for the thermoelectric properties of a single junction and their dependence on the doping concentration of the silicon nanoparticles. Finally, we discuss the thermoelectric figure of merit *ZT* of a 3D array of molecular junctions.

II. THEORY

A. *ZT* and power factor of an array of molecular junctions

As shown in Fig. 1, the molecular-junction array is made up of *n*-doped silicon nanoparticles in the shape of cubes (100 nm in size) with {100} surfaces where the nanoparticles are interconnected by bridging molecules (~ 3 nm in length) which form the molecular junctions. Neighboring bridging molecules are sufficiently far apart such that electron and phonon transfer between molecules cannot take place. In addition to the bridging molecules there are short polar molecules attached to the silicon nanoparticle surfaces as shown in Figs. 1 and 2. The polar molecules are too short to bridge the silicon nanoparticles. The role of the polar molecules is (a) to suppress band bending in the *n*-doped silicon nanoparticles and (b) to shift the highest occupied molecular orbital (HOMO) resonances of the bridging molecules upward such that some of the molecular resonances are slightly above the conduction band edge of the silicon nanoparticles. This guarantees a large electrical conductance of the bridging molecules which is a necessary requirement to obtain a large

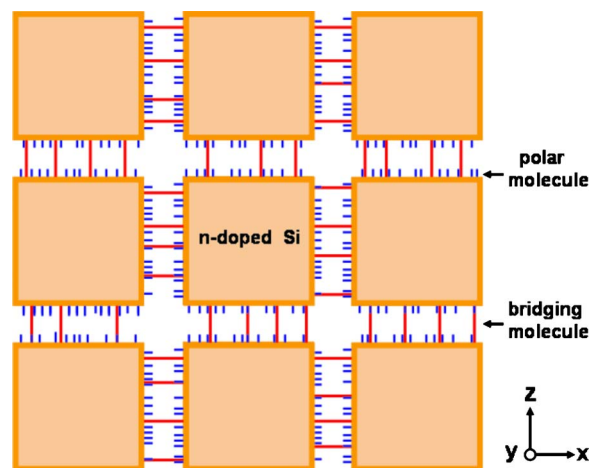


FIG. 1. (Color online) Schematic of a part of a 3D array of molecular junctions which consists of cubes of *n*-doped silicon nanoparticles 100 nm in size that are bridged by molecules (~ 3 nm long) which form the junctions. The nanoparticle surfaces are partially covered by short polar molecules. The array structure of cubic nanoparticles is repeated along the *y*-direction. The schematic shown is not to scale.

thermoelectric figure of merit *ZT* and a large power factor. The suppression of the band bending and the shift of the molecular resonances are schematically indicated in Fig. 3. In a 100 nm *n*-doped silicon nanoparticle, due to its small size, any band bending can be expected to be much smaller than that near the surface of doped bulk silicon. Also, in a realistic case, due to imperfections, the polar-molecule-surface coverage will be less than 100%.

The directions of the temperature gradient and of the electronic current flow are chosen along the *x*-direction of the molecular-junction array (Fig. 1) and therefore only molecular junctions that connect nanoparticles along the *x*-direction are of relevance when calculating the thermoelectrics of the molecular-junction array. According to Fig. 1, the array can be thought of as being made up of equal building blocks (BBs), each BB consisting of a single nanoparticle in series with a single molecular junction. If there are N_x , N_y , and N_z of such BBs along the *x*-, *y*-, and *z*-directions, respectively, then the electrical and thermal conductances *G* and κ of the array are given by

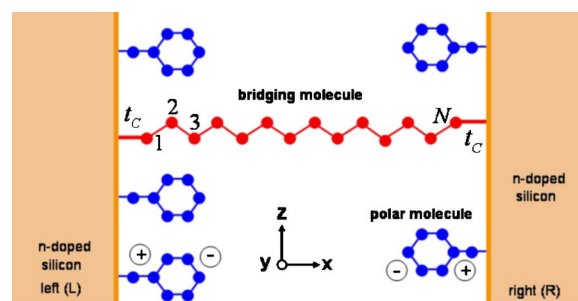


FIG. 2. (Color online) Schematic of a molecule bridging two *n*-doped Si nanoparticles on the left and right with polar molecules attached to the left and right surfaces. The carbon atoms of the bridging molecule are labeled 1 to *N*. The charges on the polar molecules are indicated. The polar molecule drawing is meant as a generic representation.

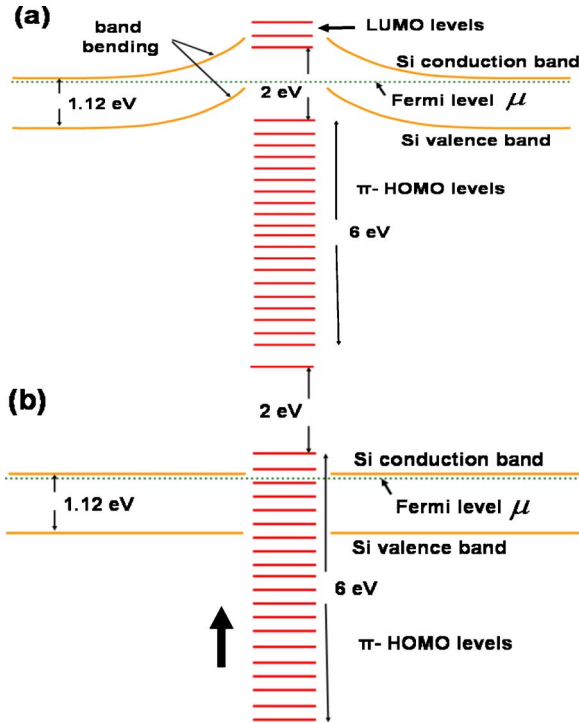


FIG. 3. (Color online) Schematic of electronic energy levels of an $N=20$ bridging molecule sandwiched between two n -doped silicon nanoparticles. (a) The system shows band bending when no polar molecules are present on the surface of the silicon nanoparticles. The Fermi level is assumed to be located in the middle of the HOMO-LUMO gap. (b) Polar molecules on the surface of the silicon nanoparticles shift the electronic levels of the bridging molecule upward (arrow) such that some HOMO resonances are above the conduction band edge of the silicon nanoparticles. The band bending is assumed to be completely suppressed by the presence of polar molecules.

$$G = \frac{N_y N_z}{N_x} G_{BB} \quad \text{and} \quad \kappa = \frac{N_y N_z}{N_x} \kappa_{BB}, \quad (4)$$

where G_{BB} and κ_{BB} are the electrical and thermal conductances of a single BB. For the array's Seebeck coefficient S one finds $S = S_{BB}$, where S_{BB} is the Seebeck coefficient of a single BB. With Eqs. (2) and (4), the figure of merit ZT of the array can be expressed solely in terms of the thermoelectric properties of its BBs, i.e.,

$$ZT = \frac{S_{BB}^2 G_{BB}}{\kappa_{BB}} T. \quad (5)$$

The power factor is given by

$$P = S_{BB}^2 G_{BB} / l, \quad (6)$$

where l is the nanoparticle size. The same formulas for ZT and P also hold for two-dimensional (2D) and one-dimensional (chain) arrays. Because a BB consists of a single nanoparticle and single molecular junction in series, it follows that

$$S_{BB} = (S_n / \kappa_n + S_j / \kappa_j) / (\kappa_n^{-1} + \kappa_j^{-1}), \quad (7)$$

$$G_{BB} = G_n G_j / (G_n + G_j), \quad (8)$$

and

$$\kappa_{BB} = \kappa_n \kappa_j / (\kappa_n + \kappa_j), \quad (9)$$

where the subscript n refers to a single nanoparticle and J to a single molecular junction. Since the nanoparticles are quite large the values for G_n and κ_n can be equated to those of bulk n -doped silicon. In the case that $G_j \ll G_n$ and $\kappa_j \ll \kappa_n$ one finds that the thermoelectric figure of merit ZT only depends on the properties of the molecular junction and

$$ZT \approx \frac{S_j^2 G_j}{\kappa_j} T. \quad (10)$$

The electrical and thermal conductances G_j and κ_j as well as the Seebeck coefficient S_j of the junctions can be expressed in terms of the individual bridging molecules of a junction. In the case that a junction contains M bridging molecules (acting in parallel), one finds

$$S_j = \frac{\sum_{i=1}^M S_i G_i}{\sum_{i=1}^M G_i}, \quad (11)$$

$$G_j = \sum_{i=1}^M G_i, \quad (12)$$

and

$$\kappa_j = \sum_{i=1}^M \kappa_i. \quad (13)$$

Here S_i , G_i , and κ_i are the Seebeck coefficient, the electrical conductance, and the thermal conductance of the i th bridging molecule, respectively. Equations (11)–(13) were derived using a classical treatment, assuming that the bridging molecules are sufficiently far apart such that quantum interference effects between conduction electrons from neighboring bridging molecules can be neglected.¹² If a_b is the average separation of bridging molecules and λ_0 the wavelength of electrons in the conduction band of the nanoparticles, then $a_b \gg \lambda_0/2$ has to be satisfied in order to justify a classical treatment. In the case of n -doped silicon, λ_0 is determined by the location of the energy pockets for the conduction band in k -space. In our case $\lambda_0 = a_l / 0.85$, where a_l is the lattice constant of silicon. When we calculate ZT later in Sec. III E, we use $M < 1000$, and the average separation between bridging molecules is sufficient to use Eqs. (11)–(13) as an approximation.

B. Thermoelectrics of a single bridging molecule

In order to derive equations for the thermoelectric properties in the i th bridging molecule of a molecular junction we employ the nonequilibrium Green's function theory. Assuming noninteracting electrons inside the nanoparticles and on the bridging molecule, one finds for the electrical current I_e of the i th bridging molecule sandwiched between two nanoparticles:¹⁷

$$I_e = \frac{2e}{h} \int d\varepsilon t_i(\varepsilon)[f_L(\varepsilon) - f_R(\varepsilon)]. \quad (14)$$

Here e is the electron charge ($e < 0$), h is the Planck constant, $t_i(\varepsilon)$ is the transmission coefficient of the i th bridging molecule, and $f_{L/R}(\varepsilon)$ are the electron Fermi distributions in the left (L) and right (R) nanoparticles. The factor of 2 in Eq. (14) accounts for the two spin states allowed for an electron in each energy level ε . Equation (14) was originally derived for macroscopic electrodes¹⁷ but it still holds in the case of our nanoparticles as the nanoparticles are sufficiently large in size such that the electronic energy level spacing as well as the Coulomb charging energy are small compared to the thermal energy kT at room temperature (k is the Boltzmann factor).

Assuming that the thermal and electrical conductances of a molecular junction are small compared to those of a nanoparticle ($\kappa_j \ll \kappa_n$; $G_j \ll G_n$), the chemical potentials $\mu_{L/R}$ as well as the temperatures $T_{L/R}$ are approximately uniform within each nanoparticle, and the chemical potential difference $\Delta\mu = \mu_L - \mu_R$ and the temperature difference $\Delta T = T_L - T_R$ thus only occur across the molecular junctions along the x -direction. Taking ΔT and $\Delta\mu$ sufficiently small, one can write, using a Taylor expansion,

$$f_L(\varepsilon) - f_R(\varepsilon) = \frac{\partial f(\varepsilon)}{\partial \mu} \Delta\mu + \frac{\partial f(\varepsilon)}{\partial T} \Delta T. \quad (15)$$

Here $f(\varepsilon)$ is the electron Fermi distribution

$$f(\varepsilon) = (1 + e^{(\varepsilon - \mu)/kT})^{-1}. \quad (16)$$

Since $\Delta\mu$ and ΔT are infinitesimal we have $\mu = \mu_L$ and $T = T_L$.

Similar to Eq. (14), the thermal current I_Q is defined as

$$I_Q = \frac{2}{h} \int d\varepsilon (\varepsilon - \mu) t_i(\varepsilon) [f_L(\varepsilon) - f_R(\varepsilon)]. \quad (17)$$

The difference between Eqs. (14) and (17) is that the electron charge e in Eq. (14) is replaced in Eq. (17) by the electron kinetic energy, $\varepsilon - \mu$, relative to the Fermi level μ . By using Eqs. (14)–(17) one finds^{12,18,19}

$$\begin{pmatrix} I_e \\ I_Q \end{pmatrix} = \begin{pmatrix} e^2 L_0 & e L_1 \\ e L_1 & L_2 \end{pmatrix} \begin{pmatrix} \Delta V \\ \Delta T/T \end{pmatrix}, \quad (18)$$

where $\Delta V = \Delta\mu/e$ is the voltage drop across a molecular junction and L_m with $m=0, 1, 2$ is defined as

$$L_m = \frac{2}{h} \int d\varepsilon t_i(\varepsilon) \left(-\frac{\partial f}{\partial \varepsilon} \right) (\varepsilon - \mu)^m. \quad (19)$$

Using Eq. (18) one can derive expressions for the Seebeck coefficient S_i , the electrical conductance G_i , and the electronic thermal conductance $\kappa_{e,i}$ of the i th bridging molecule in terms of the L_m . One finds, using the definitions for S_i , G_i , and $\kappa_{e,i}$,¹²

$$S_i \equiv - \left. \frac{\Delta V}{\Delta T} \right|_{I_e=0} = \frac{1}{eT} \frac{L_1}{L_0}, \quad (20)$$

$$G_i \equiv \left. \frac{I_e}{\Delta V} \right|_{\Delta T=0} = e^2 L_0, \quad (21)$$

$$\kappa_{e,i} \equiv \left. \frac{I_Q}{\Delta T} \right|_{I_e=0} = \frac{L_2 - L_1^2/L_0}{T}. \quad (22)$$

The quantities S_i , G_i , and $\kappa_{e,i}$ (together with $\kappa_{ph,i}$) can then be used to calculate the thermoelectric figure of merit ZT and the power factor using Eqs. (5)–(9) and (11)–(13).

1. Transmission coefficient

In order to calculate the L_m of Eq. (19), the transmission coefficient $t_i(\varepsilon)$ of the i th bridging molecule has to be calculated. Using the nonequilibrium Green's function technique one finds^{17,20}

$$t_i(\varepsilon) = 4 \text{Tr} \{ \text{Im} \Sigma_L(\varepsilon) \mathcal{G}^+(\varepsilon) \text{Im} \Sigma_R(\varepsilon) \mathcal{G}(\varepsilon) \}, \quad (23)$$

where Tr is the trace, $\Sigma_{L/R}(\varepsilon)$ are the self-energies of the left (L) and right (R) nanoparticles, and $\mathcal{G}(\varepsilon)$ is the Green's function operator, describing electron propagation along the i th bridging molecule, where

$$\mathcal{G}(\varepsilon) = (\varepsilon - \mathcal{H} - \Sigma_L - \Sigma_R)^{-1}. \quad (24)$$

Here \mathcal{H} is a single electron Hamiltonian describing the i th bridging molecule and its electrostatic interaction with the polar surface molecules. For \mathcal{H} we use a simple tight-binding Hamiltonian where a single electronic orbital $|n\rangle$ with $n = 1, 2, \dots, N$ is assigned to each of the N carbon atoms of a bridging molecule (see Fig. 2) assuming that the $|n\rangle$ states are orthogonal. The tight-binding Hamiltonian has the form

$$\begin{aligned} \mathcal{H} = & \sum_n (\varepsilon_B + e\Phi_n) |n\rangle \langle n| + t_B \\ & \times \left[\sum_{n=1}^{N-1} |n\rangle \langle n+1| + \sum_{n=2}^N |n-1\rangle \langle n| \right], \end{aligned} \quad (25)$$

where $\varepsilon_B + e\Phi_n$ are the on-site energies and t_B is the nearest neighbor transfer integral. The quantity Φ_n is the electrostatic potential generated at site n of the i th bridging molecule by the polar molecules that partially cover the surfaces of adjacent silicon nanoparticles, and ε_B are the on-site energies if $\Phi_n = 0$. The electrostatic potential Φ_n depends on the local polar molecule environment which for a coverage of less than 100% is somewhat different for each bridging molecule in the junction.

Along a polyacetylene bridging molecule, only the carbon atom sites are considered as they form the bridge along which electrons propagate, and the $|n\rangle$ states thus represent π -orbitals. Most of our calculations were done for $N=20$. In this case we take the HOMO-LUMO (lowest unoccupied molecular orbital) gap of the *trans*-polyacetylene as 2 eV and the valence π -band width as 6 eV.²¹ This value for the valence π -band width means that the tight-binding transfer integral is $t_B = -1.5$ eV. We assume that without polar molecules the Fermi level is located in the middle of the HOMO-LUMO gap which results in $\varepsilon_B - \mu = -4$ eV. (This assumption is not critical to our model, and any position of the Fermi level within the HOMO-LUMO gap could have

been chosen without changing the essential results of our calculations.) This fixes the parameters ε_B and t_B of the tight-binding Hamiltonian in Eq. (25).

Using the Hamiltonian of Eq. (25) and assuming that the bridging molecule is tethered in the same way at both its ends to the silicon nanoparticles, one obtains for the transmission coefficient $t_i(\varepsilon)$ of Eq. (23) (Refs. 22 and 23)

$$t_i(\varepsilon) = 4(\text{Im}\langle 1|\Sigma_L(\varepsilon)|1\rangle)^2 |\langle 1|\mathcal{G}(\varepsilon)|N\rangle|^2. \quad (26)$$

In order to calculate the matrix element $\langle 1|\mathcal{G}(\varepsilon)|N\rangle$ one has to determine the inverse of a complex $N \times N$ matrix with matrix elements $\langle n|\varepsilon - \mathcal{H} - \Sigma_L(\varepsilon) - \Sigma_R(\varepsilon)|m\rangle$ where $n=1, 2, \dots, N$ and $m=1, 2, \dots, N$. In our model calculation we neglect any possible dissipative electron-phonon scattering along the bridging molecules.

2. Self-energy

To determine the transmission coefficients $t_i(\varepsilon)$ given by Eq. (26), the self-energy matrix element $\langle 1|\Sigma_L(\varepsilon)|1\rangle$, which is equal to $\langle N|\Sigma_R(\varepsilon)|N\rangle$, has to be calculated. The self-energy matrix element $\langle 1|\Sigma_L(\varepsilon)|1\rangle$ is defined as

$$\langle 1|\Sigma_L(\varepsilon)|1\rangle = \sum_{\vec{k}, \sigma \in L} \frac{\langle 1|V|\psi_{\vec{k}, \sigma}\rangle \langle \psi_{\vec{k}, \sigma}|V|1\rangle}{\varepsilon - \varepsilon_{\vec{k}} + i\zeta}, \quad (27)$$

where $\zeta > 0$ is infinitesimal. Here the quantity V is the interaction of the bridging molecule with the silicon surface at the point where the bridging molecule is tethered to the surface. The symbol $|\psi_{\vec{k}, \sigma}\rangle$ is the Bloch wave function for the left silicon nanoparticle, where \vec{k} is the Bloch wave vector, σ the electron spin, and $\varepsilon_{\vec{k}}$ is the electron dispersion relation for the nanoparticle. We write the Bloch wave function of the left nanoparticle as

$$|\psi_{\vec{k}, \sigma}\rangle = \sqrt{\frac{2}{\nu}} \sum_{j, \sigma} e^{i\vec{k} \cdot \vec{R}_{j, \perp}} \sin(k_x R_{j, x}) |\varphi_{j, \sigma}\rangle, \quad (28)$$

where ν is the number of primitive cells in the left nanoparticle, \vec{R}_j are the Bravais lattice positions, and $|\varphi_{j, \sigma}\rangle$ are the on-site electronic orbitals. The index \perp refers to the transverse directions. In contrast to a Bloch state in an infinite crystal, the function $\sin(k_x R_{j, x})$ in Eq. (28) ensures that the Bloch wave vanishes at the nanoparticle surface. By using Eqs. (27) and (28) one derives for the imaginary part of the self-energy matrix element $\langle 1|\Sigma_L(\varepsilon)|1\rangle$ the expression

$$\text{Im}\langle 1|\Sigma_L(\varepsilon)|1\rangle = -\frac{2\pi}{\nu} t_c^2 \sum_{\vec{k}} \sin^2(k_x a_l/2) \delta(\varepsilon - \varepsilon_{\vec{k}}), \quad (29)$$

where a_l is the lattice parameter of silicon, $a_l = 0.357$ nm, and $t_c = \langle 1|V|\varphi_{j=0, \sigma}\rangle$ is the coupling of the end-atom of the molecular bridge to a surface atom [$j=0$ in Eq. (28)] of the silicon nanoparticle. For the electron dispersion relation of the semiconductor nanoparticles $\varepsilon_{\vec{k}}$, we use the parabolic conduction band approximation. In the first Brillouin zone, silicon has six ellipsoidal energy pockets¹⁹ centered at $|k_0| = 0.85 \cdot 2\pi/a_l$ along the k_x , k_y , and k_z directions. For the two pockets along the k_x direction the electron energy dispersion is

$$\varepsilon_{\vec{k}} = \frac{\hbar^2}{2m_l} (k_x \pm k_0)^2 + \frac{\hbar^2}{2m_t} k_y^2 + \frac{\hbar^2}{2m_t} k_z^2 + \varepsilon_{cb}, \quad (30)$$

where ε_{cb} is the conduction band edge. Similar expressions hold for the other four energy pockets along the k_y and k_z directions. In the case of silicon, the longitudinal and transverse electron masses are $m_l = 0.98m_0$ and $m_t = 0.19m_0$, respectively, where m_0 is the bare electron mass. By using Eqs. (29) and (30) one derives for $\text{Im}\langle 1|\Sigma_L(\varepsilon)|1\rangle$ the expression

$$\begin{aligned} \text{Im}\langle 1|\Sigma_L(\varepsilon)|1\rangle = & -\frac{t_c^2}{4\pi\hbar^2} a_l^3 \left\{ m_l \left[2 \sqrt{\frac{2m_l}{\hbar^2}(\varepsilon - \varepsilon_{cb})} \right. \right. \\ & \left. \left. - \frac{2}{a_l} \cos(k_0 a_l) \sin\left(a_l \sqrt{\frac{2m_l}{\hbar^2}(\varepsilon - \varepsilon_{cb})} \right) \right] \right. \\ & \left. + (m_l m_t)^{1/2} \left[4 \sqrt{\frac{2m_t}{\hbar^2}(\varepsilon - \varepsilon_{cb})} \right. \right. \\ & \left. \left. - \frac{4}{a_l} \sin\left(a_l \sqrt{\frac{2m_t}{\hbar^2}(\varepsilon - \varepsilon_{cb})} \right) \right] \right\} \quad (31) \end{aligned}$$

for $\varepsilon \geq \varepsilon_{cb}$ and $\text{Im}\langle 1|\Sigma_L(\varepsilon)|1\rangle = 0$ for $\varepsilon < \varepsilon_{cb}$. Calculating the real part of $\langle 1|\Sigma_L(\varepsilon)|1\rangle$ around the conduction band edge ε_{cb} , one finds a very weak dependence on ε and thus the real part of $\langle 1|\Sigma_L(\varepsilon)|1\rangle$ has the effect of causing a constant shift of the on-site energies of atom 1 and atom N of the bridging molecule.^{20,24} We neglect this effect in our calculations and set $\text{Re}\langle 1|\Sigma_L(\varepsilon)|1\rangle = 0$. Just above the conduction band edge $-\text{Im}\langle 1|\Sigma_L(\varepsilon)|1\rangle$ follows a $\sqrt{\varepsilon - \varepsilon_{cb}}$ behavior.

The tethering of the bridging molecule to the nanoparticle surfaces and thus the coupling parameter t_c can be tuned by chemical means, i.e., by changing the bridging molecules end atoms or choosing particular bonding sites (top or hollow sites)²⁵ on the silicon nanoparticle surfaces.

3. Bridging molecule/polar molecule interaction

The electrostatic potential Φ_n acts upon a bridging molecule like a ‘‘gate voltage’’ and is given by

$$\begin{aligned} \Phi_n = & \frac{p}{4\pi\varepsilon_0\varepsilon_r d} \left\{ \sum_{j, \text{occ. left}} \left[\frac{1}{|\vec{r} - \vec{r}_j|} - \frac{1}{|\vec{r} - (\vec{r}_j + \vec{d})|} \right] \right. \\ & \left. + \sum_{j, \text{occ. right}} \left[\frac{1}{|\vec{r} - (\vec{r}_j + \vec{L})|} - \frac{1}{|\vec{r} - (\vec{r}_j + \vec{L} - \vec{d})|} \right] \right\}. \quad (32) \end{aligned}$$

The quantity p is the dipole moment of a single polar molecule, $\vec{d} = d\vec{e}_x$ (see Fig. 2) where d is the length of the dipole and \vec{e}_x the unit vector in x -direction, ε_r is the relative permittivity of a polar molecule, and ε_0 is the vacuum permittivity. The \vec{r}_j 's are the occupied 2D square-lattice sites on the nanoparticle surfaces left and right of a junction. The quantity \vec{r} denotes the carbon-atom positions on the bridging molecule. If one neglects the transverse positional components of the carbon atoms, one has $\vec{r} = na_0\vec{e}_x$ where $n=1, 2, \dots, N$ and a_0 is the spacing between carbon atoms along the x direction. $\vec{L} = (N+1)a_0\vec{e}_x$ is the width of the molecular junction where for simplicity it is assumed that the end-atom-to-surface bond length is equal to a_0 . Equation (32) does not include the

effect of an image potential caused by the electronic polarization of the silicon nanoparticles induced by the polar molecules. We have investigated the effect of the image potential by employing the method of image charges.^{26,27} We found that in our case the image potential reduces Φ_n of Eq. (32) predominantly near the end atoms of a bridging molecule and less so in the center where the reduction is less than 10%. Also, the image potential did not change the fluctuating nature of the Φ_n 's, which shifts the electronic levels of the bridging molecules in a statistical manner. For simplicity we thus neglected the image potential in our calculation.

C. Phononic thermal conductance

For individual molecules the familiar concept of heat transport no longer applies as the energy is carried by discrete vibrational excitations. The phononic thermal conductance $\kappa_{ph,i}$ of a bridging molecule will depend on its vibrational spectrum, on the vibrational spectrum of the silicon nanoparticles, and on the values of the bending force and stretching force constants of the bonds that tether the end atoms of the bridging molecule to the silicon surfaces. The tethering could be optimized to minimize $\kappa_{ph,i}$. In this paper we have made no attempt to calculate $\kappa_{ph,i}$. Instead, we assume that the $\kappa_{ph,i}$ are the same for all the bridging molecules and we investigate the thermoelectric figure of merit ZT as a function of $\kappa_{ph,i}$ in the range from $\kappa_{ph,i}=10^{-14}$ W/K to $\kappa_{ph,i}=10^{-10}$ W/K. Segal *et al.* have performed microscopic calculations for the phononic heat transport through molecular chains that connect two thermal reservoirs. Depending on the Debye frequency of the reservoirs and on the molecule-reservoir coupling, Segal *et al.*²⁸ found values for $\kappa_{ph,i}$ of an alkane chain with $N=20$ at room temperature between 2×10^{-13} and 3×10^{-11} W/K. A classical heat conduction model, where the molecule resembles a cylindrical volume and where the heat conductivity is that of typical bulk organic solids, was found to overestimate the microscopic result by about one order of magnitude. Recently, Wang *et al.*²⁹ have measured the thermal conductance of long alkane molecules in a monolayer attached to a gold surface and found a value of $\kappa_{ph,i}=5 \times 10^{-11}$ W/K.

III. RESULTS AND DISCUSSIONS

There are seven parameters in our model. These seven parameters are (1) the number N of carbon atoms that form the bridging molecule, (2) the position of the Fermi level μ relative to the conduction band edge ε_{cb} of the silicon nanoparticles (μ can be varied by changing the n -doping concentration), (3) the coupling strength t_c between a silicon atom on the $\{100\}$ silicon surface and the atom at the ends of the bridging molecule, assuming that the tethering can be tuned by chemical means, (4) the dipole moment p/ε_r of the polar molecules that partially cover the nanoparticle surfaces, (5) the length d of the dipoles, (6) the coverage ξ of the polar molecules, and (7) the phononic thermal conductance $\kappa_{ph,i}$ of a bridging molecule. All the calculations were done for room temperature, i.e., at $T=300$ K.

A. Shifting the HOMO levels

There are two reasons for partially covering the surfaces of the silicon nanoparticles with polar molecules: First, polar molecules attached to the surfaces of the n -doped silicon nanoparticles can strongly reduce band bending as shown experimentally by Cohen *et al.*³⁰ for polar molecules assembled on an n -doped (100) silicon surface. In our model we make the assumption that the presence of polar molecules on the surface completely eliminates any band bending. Second, the polar molecules produce an electrostatic potential Φ_n at each atom site n along the bridging molecules which causes the energy levels of the bridging molecules to shift upward such that some of the upper HOMO levels (π -valence band of *trans*-polyacetylene) shift above the conduction band edge ε_{cb} of the semiconductor nanoparticles. The elimination of band bending and the shifting of the HOMO levels are indicated schematically in Figs. 3(a) and 3(b). The amount of level shifting depends on the strength of the dipole moment p/ε_r as well as on the details of the site-occupation configuration of the polar molecules in the vicinity of the bridging molecules.

B. Polar molecule site-occupation fluctuations

The polar molecules supply a gate voltage Φ_n to the bridging molecules, which affects the location of the resonance levels of the bridging molecules relative to the conduction band edge ε_{cb} of the silicon nanoparticles. In the case of partial surface coverage with polar molecules, each bridging molecule has a different polar-molecule neighborhood and thus the electrostatic potential Φ_n does fluctuate from one bridging molecule to the next. We assume that M bridging molecules are placed at random in a junction, connecting binding sites on 2D square lattices of the left and right junction surfaces. The 2D square-lattice parameter was chosen to be equal to the dimer-row separation on a Si(100)- 2×1 reconstructed surface, i.e., $a_s=0.77$ nm. Thus the "footprint" of a polar molecule or a bridging molecule is a_s^2 . The procedure we adopted to calculate Φ_n in Eq. (32) was the following. A bridging molecule was placed into an infinite junction and connected to the left and right surfaces at $(x,y,z)=(0,0,0)$ and $((N+1)a_0,0,0)$. (Since the width of a junction is much smaller than the nanoparticle size and because of the regular junction array structure shown in Fig. 1, assuming an infinite junction is a good approximation.) Using a random number generator, polar molecules were placed randomly left and right onto the 2D lattice sites within a radius of $r_0=200a_s$ until the coverage ξ was reached. The small additional contribution to Φ_n from outside r_0 to infinity was obtained by using an analytical expression where the charges on the polar molecules were approximated by parallel continuous charge layers of zero thickness. Figure 4 shows $e\Phi_n$ for 300 bridging molecules that were sampled versus the position at atom site n along the bridging molecules for coverage $\xi=0.4, 0.7$, and 1.0 with $N=20$, $p/\varepsilon_r=6$ D, (1 D = 1 Debye = 3.34×10^{-30} C m), and $d=2.5a_0$ ($a_0=0.122$ nm). The vertical bars indicate the size of the fluctuations in Φ_n . For illustration, the two full lines in Fig. 4, for coverages $\xi=0.4$ and 0.7, connect the $e\Phi_n$'s that belong to

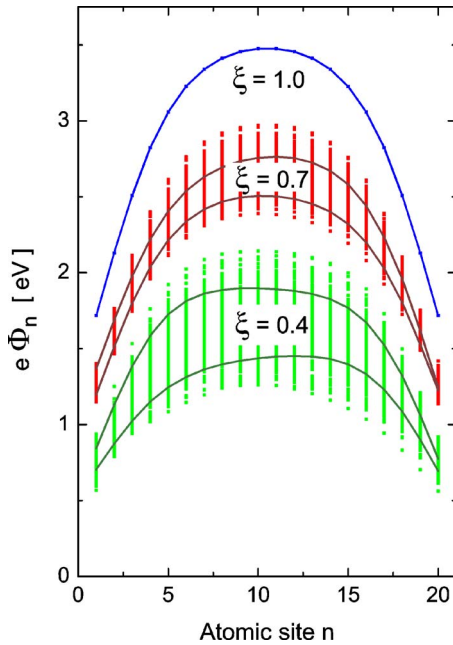


FIG. 4. (Color online) Electrostatic potential energy $e\Phi_n$ [Eq. (32)] at atom site n of *trans*-polyacetylene ($N=20$) bridging molecules in a junction. Here $p/\epsilon_r=6$ D (1 D=1 Debye= 3.34×10^{-30} C m) and the polar-molecule dipole length is $d=2.5a_0$. The polar-molecule coverages used are $\xi=0.4, 0.7$, and 1.0 . The vertical bars indicate the fluctuation ranges of $e\Phi_n$ where 300 bridging molecules were sampled. In the case of $\xi=0.4$ and 0.7 , the two solid lines connect $e\Phi_n$'s of two bridging molecules randomly selected from the sample of 300 molecules.

two bridging molecules that were randomly chosen from the 300 ones that were sampled. Figure 4 reveals that the relative $e\Phi_n$ fluctuations decrease with increasing polar-molecule coverage ξ and that the fluctuations become very small when the coverage ξ approaches 1. As can be seen in Fig. 4, $e\Phi_n$ increases within the left and right polar-molecule layers of thickness $d=2.5a_0$ and in the middle part of a bridging molecule reaches a value of $e\Phi_n \approx |e|\xi p/(\epsilon_0\epsilon_r a_s^2)$. Calculating the position of the resonances of the bridging molecules by using Eq. (26), we found that in the case of coverage $\xi=0.7$, the HOMO resonances of all the 300 sampled bridging molecules were shifted sufficiently upward such that upper HOMO resonances became located above the conduction band edge ϵ_{cb} . In contrast, in the case of coverage $\xi=0.4$, the highest HOMO resonance was not always shifted above ϵ_{cb} . In a realistic case it will be difficult to achieve perfect polar molecule coverage due to surface imperfections and nanoparticle edge effects. Therefore, in what follows, the coverage $\xi=0.7$ instead of $\xi=1$ was chosen. (Also, due to the procedure we adopted to calculate Φ_n , the case $\xi=1$ is unusual as for $\xi \rightarrow 1$ the fluctuations in Φ_n vanish and the electronic level positions of all the bridging molecules become the same. In this case ZT shows strong oscillating behavior as a function of the polarization p of the polar molecules as the resonances of the bridging molecules move collectively across the conduction band edge.)

C. Transmission coefficients of bridging molecules

As an example, Fig. 5 depicts three different transmission coefficients $t_i(\epsilon)$ versus $(\epsilon - \mu)/kT$ of three bridging

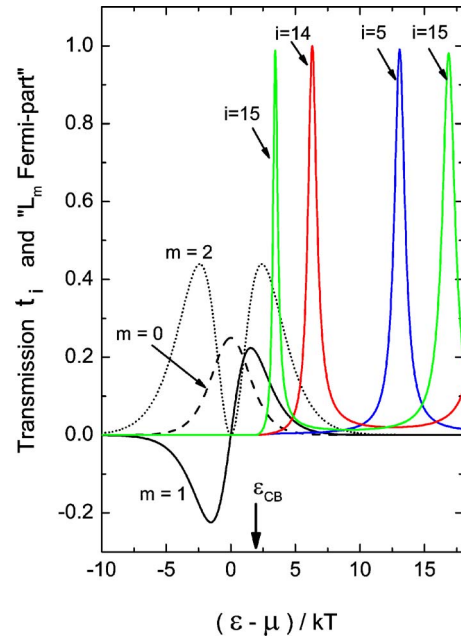


FIG. 5. (Color online) Transmission coefficients $t_i(\epsilon)$ and the “Fermi part” of L_m [integrand without $t_i(\epsilon)$] for $m=0, 1$, and 2 vs $(\epsilon - \mu)/kT$. The transmission coefficients $t_i(\epsilon)$ chosen at random from the sample of 300 are those for the bridging molecules labeled $i=5, 14$, and 15 . The parameters are $N=20$, $t_c=-2$ eV, $\mu=\epsilon_{cb}-2kT$, $p/\epsilon_r=6$ D, $d=2.5a_0$, $\xi=0.7$, and $T=300$ K.

molecules ($i=5, 14, 15$) that were randomly selected from the 300 ones that were sampled. Also displayed in Fig. 5 are $(-\partial f/\partial \epsilon)(\epsilon - \mu)^m$ for $m=0, 1$, and 2 which are the “Fermi parts” in the integrand of L_m as defined in Eq. (19). The position of the Fermi level is chosen as $\mu=\epsilon_{cb}-2kT$ which corresponds to an n -doping concentration of about 3×10^{18} cm^{-3} . Figure 5 reveals that in our case only a single resonance of $t_i(\epsilon)$, the one closest to and above ϵ_{cb} , contributes to the thermoelectric properties. As can be seen in Fig. 5, the width of the contributing resonance in $t_i(\epsilon)$ increases the further the resonance is away from the conduction band edge ϵ_{cb} , which is due to the fact that $-\text{Im}\langle 1|\Sigma_L(\epsilon)|1\rangle$ increases the larger $\epsilon - \epsilon_{cb}$ becomes [Eq. (31)].

D. Thermoelectrics of a junction of bridging molecules

Figure 6 shows the Seebeck coefficients S_i of 300 bridging molecules that were sampled. The model parameters chosen are given in the figure caption of Fig. 6. The figure shows that the S_i values of individual bridging molecules fluctuate between $2k/e$ (where $k/e=-86.2$ $\mu\text{V}/\text{K}$) and $6k/e$. If instead of silicon nanoparticles one would have chosen metal nanoparticles, the S_i 's would be positive as well as negative depending on the position of the main resonance of a bridging molecule relative to the Fermi level. If the resonance that is closest to the Fermi level lies above the Fermi level, then $S_i < 0$, otherwise $S_i > 0$. Therefore, it follows from Eq. (11) that for metal nanoparticles $S_j \approx 0$ which would lead to $ZT = 0$. Thus, the usage of semiconductor nanoparticles (like silicon nanoparticles) is mandatory to achieve a thermoelectric figure of merit $ZT > 0$.

By using Eqs. (11)–(13), we have calculated the thermoelectric quantities S_J , G_J , and $\kappa_{e,J}$ of a molecular junction

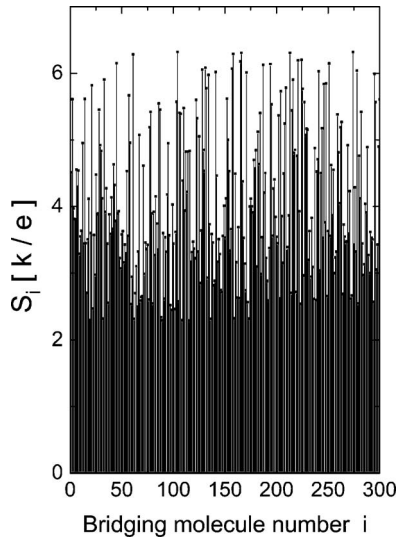


FIG. 6. Seebeck coefficients S_i in units of k/e for 300 sampled bridging molecules. The parameters are $N=20$, $t_c=-2$ eV, $\mu=\varepsilon_{cb}-2kT$, $p/\varepsilon_r=6$ D, $d=2.5a_0$, $\xi=0.7$, and $T=300$ K.

from the thermoelectric properties of its M individual bridging molecules. Figures 7 and 8 depict the Seebeck coefficient S_J , the electrical conductance G_J/M per bridging molecule, and the electronic thermal conductance $\kappa_{e,J}/M$ per bridging molecule of a junction versus the Fermi level position, i.e., $(\mu-\varepsilon_{cb})/kT$, for different coupling parameters t_c . The other parameters are given in the figure caption of Fig. 7. The sampling size of bridging molecules was 4000 which we found to result in a statistical sampling error for S_J , G_J , and κ_J of less than 2%. The investigated range of the position of the Fermi level corresponds to n -doping concentrations be-

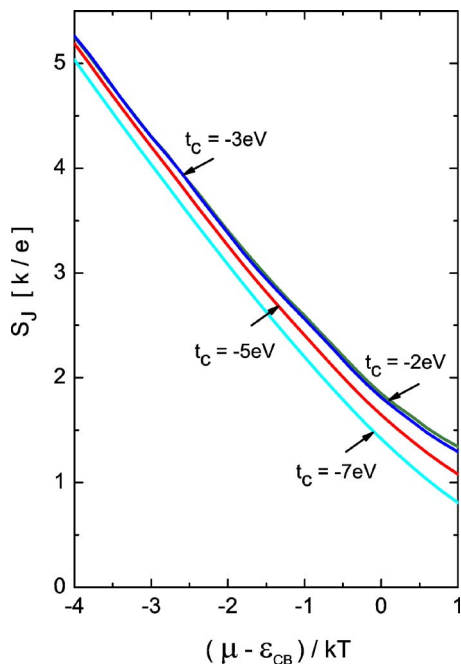


FIG. 7. (Color online) Seebeck coefficient S_J of a molecular junction as defined by Eq. (11) vs the position of the Fermi level relative to the silicon conduction band edge, i.e., $(\mu-\varepsilon_{cb})/kT$, for different coupling parameters t_c . Other parameters are $N=20$, $p/\varepsilon_r=6$ D, $d=2.5a_0$, $\xi=0.7$, and $T=300$ K. The sampling size of bridging molecules is 4000.

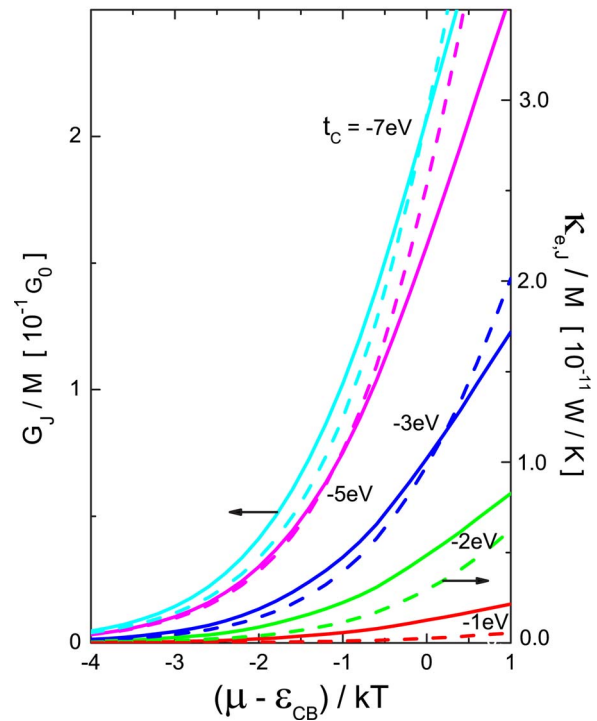


FIG. 8. (Color online) Electrical conductance G_J/M and electronic thermal conductance $\kappa_{e,J}/M$ of a junction per bridging molecule as defined by Eqs. (12) and (13) vs the position of the Fermi level relative to the silicon conduction band edge, i.e., $(\mu-\varepsilon_{cb})/kT$, for different coupling parameters t_c . Other parameters are $N=20$, $p/\varepsilon_r=6$ D, $d=2.5a_0$, $\xi=0.7$, and $T=300$ K. The sampling size of bridging molecules is 4000.

tween 3×10^{17} and about 4×10^{19} cm^{-3} . Figure 7 shows that the Seebeck coefficient of a molecular junction S_J increases the further the Fermi level drops below the conduction band edge and that S_J varies between $1k/e$ and $5k/e$. In contrast, G_J/M and $\kappa_{e,J}/M$ in Fig. 8 rapidly decrease by lowering the Fermi level. While S_J is almost independent of coupling strength t_c , the electrical conductance G_J , and the electronic thermal conductance $\kappa_{e,J}$ of a molecular junction increase with increasing t_c due to the fact that the width of the molecular resonances increases.

Figure 9 reveals that a molecular junction strongly deviates from the Wiedemann–Franz law,¹⁹ i.e., $1 = 3e^2\kappa_{e,J}/(\pi^2G_Jk^2T)$ (dotted line), which is known to be valid for a metal. As can be seen in Fig. 9, $3e^2\kappa_{e,J}/(\pi^2G_Jk^2T)$ depends only weakly on the Fermi level position but depends strongly on t_c and approaches zero as the coupling parameter t_c goes to zero.

E. ZT and power-factor of an array of molecular junctions

The thermoelectric figure of merit ZT for an array of molecular junctions is given by Eq. (5). Using the thermal conductivity value for n -doped bulk silicon measured by Brinson *et al.*,³¹ one finds that for a 100 nm sized n -doped Si nanoparticle $\kappa_J \ll \kappa_n$ even for the maximum possible number, i.e., $M \approx 40\,000$ of bridging molecules that could fit into a single junction ($\kappa_{\text{ph},i} \leq 10^{-10}$ W/K was assumed). This means that the entire temperature drop occurs across the molecular junctions and that the temperature distribution inside

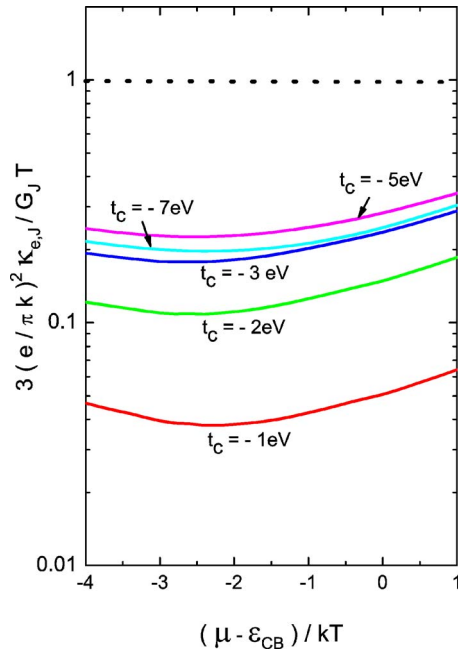


FIG. 9. (Color online) Deviation from the Wiedemann–Franz law: $3e^2\kappa_{e,j}/(\pi^2G_Jk^2T)$ vs $(\mu - \epsilon_{cb})/kT$ for different coupling parameters t_c , using the results from Fig. 8. The dashed line illustrates the value 1 corresponding to the Wiedemann–Franz law.

the silicon nanoparticles is, to a very good approximation, uniform. (This was an assumption that we had made earlier in Sec. II B when we derived the key equations that describe the thermoelectric properties of a single molecular junction.) Since $\kappa_J \ll \kappa_n$, one obtains using Eqs. (5) and (7)–(9), $ZT = S_J^2 G_{BB} T / \kappa_J$. The electrical conductance G_{BB} of the BB depends on the number M of bridging molecules in a junction. The calculations show that ZT is largest if $G_{BB} \approx G_J$, that is if $G_J \ll G_n$, which is valid for not too large values of M .

Employing Eq. (10), Figs. 10 and 11 display the thermoelectric figure of merit ZT of the molecular junction array, using the results of Figs. 7 and 8, as a function of the phononic thermal conductance $\kappa_{ph,i}$ of a single bridging molecule and of the Fermi level position $(\mu - \epsilon_{cb})/kT$. The coupling parameter is $t_c = -1$ eV (Fig. 10) and $t_c = -5$ eV (Fig. 11). The other parameters are given in the figure caption of Fig. 10. Calculating G_n and κ_n of the nanoparticles by using experimental data for the electrical and thermal conductivities of n -doped silicon^{32,31} one finds that Eq. (10) for ZT is valid as long as the number M of bridging molecules in a junction is $M < 1000$ for $t_c = -1$ eV and $M < 200$ for $t_c = -5$ eV for the doping levels shown in Figs. 10 and 11. In these M -ranges, ZT is independent of M , which follows directly from Eq. (10). The above M -ranges result from the constraint $G_J \ll G_n$, while $\kappa_J \ll \kappa_n$ is fulfilled for even larger M values. The reason that the M -range decreases with increasing $|t_c|$ is that the electrical conductance G_i of a single bridging molecule increases with coupling strength $|t_c|$. If M is greater than 1000 (or 200) one has to employ Eq. (5) for ZT instead of Eq. (10). In that case ZT is not only determined by the thermoelectric properties of the molecular junctions, i.e., S_J , G_J , and κ_J but also by S_n , G_n , and κ_n of the nanoparticles. (In the case that $G_J \gg G_n$ and $\kappa_J \gg \kappa_n$ the junctions

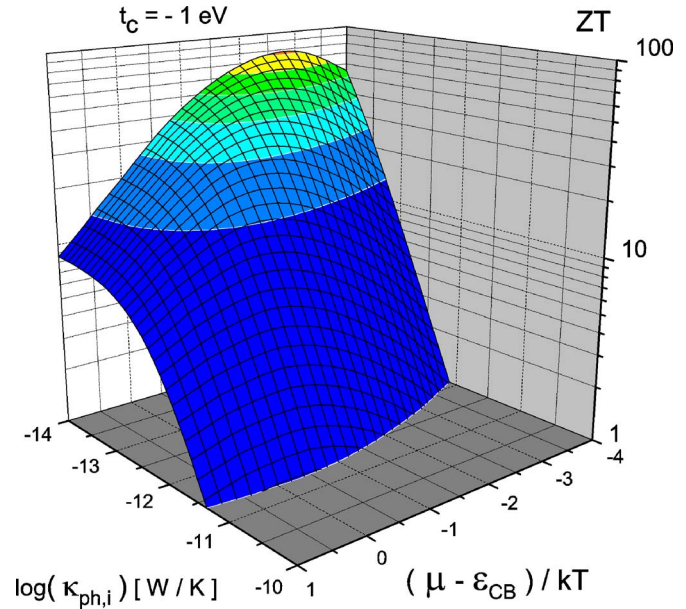


FIG. 10. (Color online) The thermoelectric figure of merit ZT of the molecular junction array as a function of the phononic thermal conductance $\kappa_{ph,i}$ of a single bridging molecule and of the Fermi level position $(\mu - \epsilon_{cb})/kT$. The coupling parameter is $t_c = -1$ eV. The other parameters are $N=20$, $M < 1000$, $p/\epsilon_r = 6$ D, $d = 2.5a_0$, $\xi = 0.7$, and $T = 300$ K.

would not play any role and ZT would be that of n -doped silicon.) Figure 10 reveals that in order to achieve $ZT > 1$ the phononic thermal conductance $\kappa_{ph,i}$ of a single bridging molecule tethered at its ends to n -doped silicon nanoparticles has to be smaller than 5×10^{-12} W/K. For the very small value of $\kappa_{ph,i} = 10^{-14}$ W/K and for a doping level corresponding to $\mu \approx \epsilon_{cb} - 2.7kT$ our model calculation predicts the very large

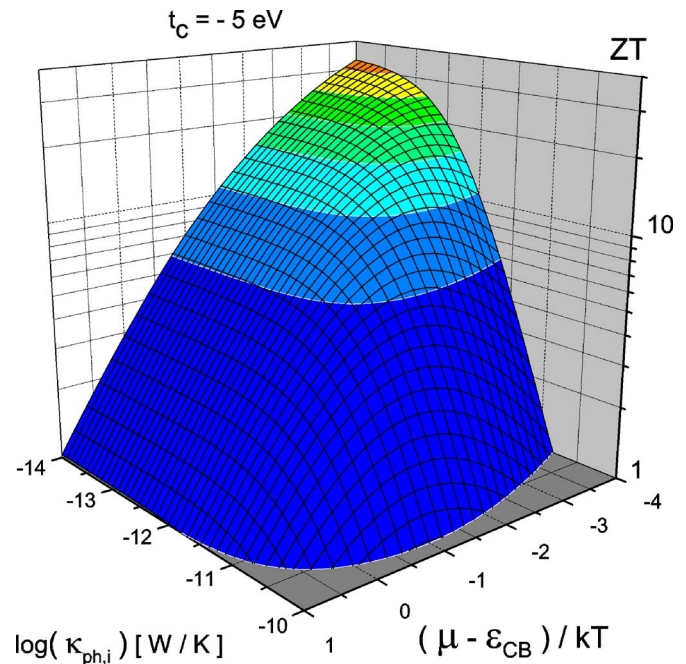


FIG. 11. (Color online) The thermoelectric figure of merit ZT of the molecular junction array as a function of the phononic thermal conductance $\kappa_{ph,i}$ of a single bridging molecule and of the Fermi level position $(\mu - \epsilon_{cb})/kT$. The coupling parameter is $t_c = -5$ eV. The other parameters are $N=20$, $M < 200$, $p/\epsilon_r = 6$ D, $d = 2.5a_0$, $\xi = 0.7$, and $T = 300$ K.

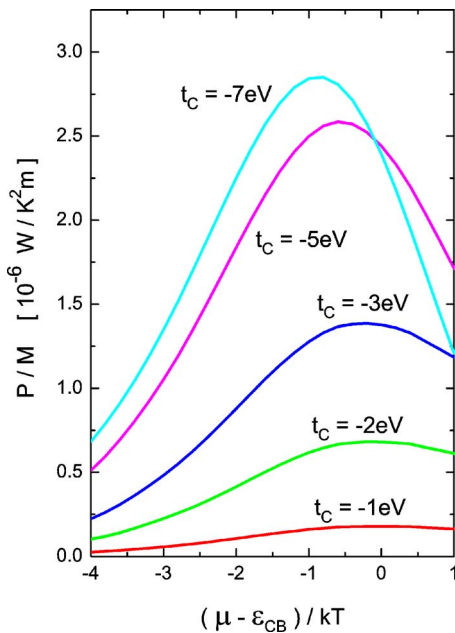


FIG. 12. (Color online) The normalized power factor P/M of an array of molecular junctions vs the Fermi level position $(\mu - \epsilon_{cb})/kT$ for different values of the coupling parameter t_c . The silicon nanoparticle size was taken as 100 nm. The other parameters are $N=20$, $p/\epsilon_r=6$, D , $d=2.5a_0$, $\xi=0.7$, and $T=300$ K.

value of $ZT \approx 80$. The situation is different in Fig. 11. Here, if the phononic thermal conductance $\kappa_{ph,i}$ of a single bridging molecule is less than 6×10^{-11} W/K, a value of $ZT > 1$ can be achieved. The large value of $ZT \approx 30$ is predicted for $\kappa_{ph,i} = 10^{-14}$ W/K and $\mu = \epsilon_{cb} - 4kT$.

The fact that large ZT values can be achieved in a 3D array of molecular junctions despite of a polar-molecule site-occupational disorder, which causes the resonances not to be placed in an optimal way, is an important result of our paper.

Segal *et al.*²⁸ have found by model calculations that the phononic thermal conductance κ_{ph} of a single alkane bridging molecule at room temperature decreases with increasing N and becomes constant for $N > 15$. Similarly, we expect that long bridging molecules have a smaller $\kappa_{ph,i}$ than shorter ones. In longer bridging molecules, the spacing $\Delta\epsilon$ between resonances becomes smaller so that the chance of a single resonance being close to the conduction band edge ϵ_{cb} is larger which leads to a high ZT value. On the other hand, if the bridging molecule becomes too long such that $\Delta\epsilon < 3kT$, more than one resonance will contribute which might decrease ZT . We also have calculated ZT for $N=30$ and $N=40$ and found similar ZT values as in the case of $N=20$.

Finally, Fig. 12 shows the power factor per junction bridging molecule, P/M , versus the Fermi level position $(\mu - \epsilon_{cb})/kT$ for different coupling parameters t_c . The power factor was calculated using the equation $P/M = S_J^2 G_J / (Ml)$ [see Eq. (6)], valid if $G_J \ll G_n$, where l is the size of the silicon nanoparticle ($l=100$ nm). Figure 12 shows that the power factor peaks at Fermi level positions between $(\mu - \epsilon_{cb})/kT = -1$ and 0. In the case of $t_c = -1$ eV, using $M=1000$, the power factor is $P \approx 2 \times 10^{-4}$ W/K² m and in the case of $t_c = -5$ eV, using $M=200$, the power factor is $P \approx 5$

$\times 10^{-4}$ W/K² m. These power factors are about ten times smaller than power factors found experimentally in conventional bismuth telluride based alloys.

IV. CONCLUSIONS

We have investigated by model calculations the thermoelectric properties of a 3D array of molecular junctions which is made of n -doped silicon nanoparticles that are bridged (as an example) by *trans*-polyacetylene molecules. We have derived formulas for the thermoelectric properties, i.e., the Seebeck coefficient S , the electrical conductance G and thermal conductance κ of the array, and its thermoelectric figure of merit ZT , and power factor P . Using nonequilibrium Green's function theory we have derived expressions for the transmission coefficient $t_i(\epsilon)$ for the individual bridging molecules of a junction. Shifting the molecular resonances of the bridging molecules by using polar surface molecules results in a large electrical conductance of the array which is essential for achieving a large ZT . In our model we assumed that material imperfections cause a partial polar-molecule-surface coverage. We have calculated the dependence of the junction thermoelectric quantities S_J , G_J , and $\kappa_{e,J}$ as a function of the n -doping concentration of the silicon nanoparticles and of the molecule-surface coupling strength t_c . A small phononic thermal conductance $\kappa_{ph,i}$ was found to be crucial in order to obtain a high ZT value ($ZT > 1$). A small $\kappa_{ph,i}$ might be achieved by optimizing the molecule-surface tethering. The calculated power factor of the array of molecular junctions was found to be lower than in conventional bismuth telluride based alloys. To make such an array of molecular junctions in practice might not be easy. We hope an array of molecular junctions can be fabricated by a self-assembly method, perhaps in a similar way as hybrid materials based on metal particles have been produced previously.^{33,34} Our model also holds for other semiconductor-nanoparticle/bridging molecule combinations, and better thermoelectric properties might be achieved with other combinations leading to even larger ZT and a larger power factor.

ACKNOWLEDGMENTS

The author acknowledges useful discussions with N. Savvides and J. Herrmann.

- ¹H. J. Goldsmid, *Thermoelectric Refrigeration* (Temple, London, 1964).
- ²G. Chen, M. S. Dresselhaus, G. Dresselhaus, J.-P. Fleurial, and T. Caillat, *Int. Mater. Rev.* **48**, 45 (2003).
- ³R. R. Heikes and R. W. Ure, *Thermoelectricity: Science and Engineering* (Interscience, New York, 1961).
- ⁴L. D. Hicks and M. S. Dresselhaus, *Phys. Rev. B* **47**, 12727 (1993).
- ⁵L. D. Hicks and M. S. Dresselhaus, *Phys. Rev. B* **47**, 16631 (1993).
- ⁶X. Sun, Z. Zhang, and M. S. Dresselhaus, *Appl. Phys. Lett.* **74**, 4005 (1999).
- ⁷Y.-M. Lin and M. S. Dresselhaus, *Phys. Rev. B* **68**, 075304 (2003).
- ⁸T. C. Harman, P. J. Taylor, M. P. Walsh, and B. E. LaForge, *Science* **297**, 2229 (2002).
- ⁹R. Venkatasubramanian, E. Siivola, T. Colpitts, and B. O'Quinn, *Nature (London)* **413**, 597 (2001).
- ¹⁰K. F. Hsu, S. Loo, F. Guo, W. Chen, J. S. Dyck, C. Uher, T. Hogan, E. K. Polychroniadis, and M. G. Kanatzidis, *Science* **303**, 818 (2004).
- ¹¹X. B. Zhao, X. H. Ji, Y. H. Zhang, J. P. Tu, and X. B. Zhang, *Appl. Phys. Lett.* **86**, 062111 (2005).

- ¹²K. Esfarjani, M. Zebarjadi, and Y. Kawazoe, *Phys. Rev. B* **73**, 085406 (2006).
- ¹³H.-K. Lyo, A. A. Khajetoorians, L. Shi, K. P. Pipe, R. J. Ram, A. Shakouri, and C. K. Shih, *Science* **303**, 816 (2004).
- ¹⁴J. R. Heath and M. A. Ratner, *Phys. Today* **56**(5), 43 (2003).
- ¹⁵P. Reddy, S.-Y. Jang, R. Segalman, and A. Majumdar, *Science* **315**, 1568 (2007).
- ¹⁶X. Zheng, W. Zheng, Y. Wei, Z. Zeng, and J. Wang, *J. Chem. Phys.* **121**, 8537 (2004).
- ¹⁷Y. Meir and N. S. Wingreen, *Phys. Rev. Lett.* **68**, 2512 (1992).
- ¹⁸U. Sivan and Y. Imry, *Phys. Rev. B* **33**, 551 (1986).
- ¹⁹N. W. Ashcroft and N. D. Mermin, *Solid State Physics* (Holt, Rinehart, and Winston, New York, 1995).
- ²⁰S. Datta, *Electronic Transport in Mesoscopic Systems* (Cambridge University Press, New York, 1995).
- ²¹V. Bezugly and U. Birkenheuer, *Chem. Phys. Lett.* **399**, 57 (2004).
- ²²V. Mujica, M. Kemp, and M. A. Ratner, *J. Chem. Phys.* **101**, 6849 (1994).
- ²³Y. Asai and H. Fukuyama, *Phys. Rev. B* **72**, 085431 (2005).
- ²⁴T. Rakshit, G.-C. Liang, A. W. Gosh, M. C. Hersam, and S. Datta, *Phys. Rev. B* **72**, 125305 (2005).
- ²⁵K.-H. Müller, *Phys. Rev. B* **73**, 045403 (2006).
- ²⁶E. Emberly and G. Kirzenow, *Ann. N.Y. Acad. Sci.* **960**, 131 (2002).
- ²⁷J. D. Jackson, *Classical Electrodynamics*, 2nd ed. (Wiley, New York, 1975), p. 132.
- ²⁸D. Segal, A. Nitzan, and P. Hänggi, *J. Chem. Phys.* **119**, 6840 (2003).
- ²⁹Z. Wang, J. A. Carter, A. Lagutchev, Y. K. Koh, N.-H. Seong, D. G. Cahill, and D. D. Dlott, *Science* **317**, 787 (2007).
- ³⁰R. Cohen, N. Zenou, D. Cahen, and S. Yitzchaik, *Chem. Phys. Lett.* **279**, 270 (1997).
- ³¹M. E. Brinson and W. Dunstan, *J. Phys. C* **3**, 483 (1970).
- ³²R. F. Pierret, *Semiconductor Device Fundamentals* (Addison-Wesley, Reading, MA, 1996).
- ³³B. Raguse, J. Herrmann, G. Stevens, J. Myers, G. Baxter, K.-H. Müller, T. Reda, A. Molodyk, and V. Braach-Maksvytis, *J. Nanopart. Res.* **4**, 137 (2002).
- ³⁴K.-H. Müller, J. Herrmann, B. Raguse, G. Baxter, and T. Reda, *Phys. Rev. B* **66**, 075417 (2002).